

Journal Pre-proofs

A modified peridynamic method to model the fracture behaviour of nanocomposites

Dayou Ma, Patricia Verleysen, Sarath Chandran, Marco Giglio, Andrea Manes

PII: S0013-7944(21)00082-5
DOI: <https://doi.org/10.1016/j.engfracmech.2021.107614>
Reference: EFM 107614

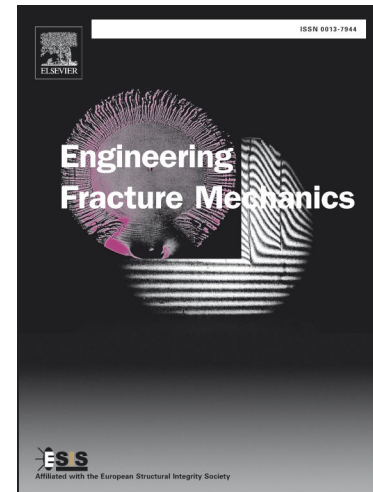
To appear in: *Engineering Fracture Mechanics*

Received Date: 28 August 2020
Revised Date: 11 February 2021
Accepted Date: 12 February 2021

Please cite this article as: Ma, D., Verleysen, P., Chandran, S., Giglio, M., Manes, A., A modified peridynamic method to model the fracture behaviour of nanocomposites, *Engineering Fracture Mechanics* (2021), doi: <https://doi.org/10.1016/j.engfracmech.2021.107614>

This is a PDF file of an article that has undergone enhancements after acceptance, such as the addition of a cover page and metadata, and formatting for readability, but it is not yet the definitive version of record. This version will undergo additional copyediting, typesetting and review before it is published in its final form, but we are providing this version to give early visibility of the article. Please note that, during the production process, errors may be discovered which could affect the content, and all legal disclaimers that apply to the journal pertain.

© 2021 Published by Elsevier Ltd.



A modified peridynamic method to model the fracture behaviour of nanocomposites

Dayou Ma^{a*}, Patricia Verleysen^b, Sarath Chandran^b, Marco Giglio^a, Andrea Manes^a

^a Politecnico di Milano, Department of Mechanical Engineering, via la Masa 1, 20156 Milan, Italy. dayou.ma@polimi.it, marco.giglio@polimi.it, andrea.manes@polimi.it

^b Department of Electromechanical, Systems & Metal Engineering, MST-DyMaLab, Ghent University, Technologiepark 46, B-9052 Zwijnaarde, Belgium. patricia.verleysen@UGent.be, sarath.chandran@UGent.be

* Corresponding author: Dayou Ma. dayou.ma@polimi.it

Abstract

In the present work, a numerical investigation based on a modified peridynamic method of fracture properties of epoxy resin reinforced by nanoparticles, more specifically hyperbranched polyester (HBP), was conducted. Due to the specific features of HBP, certain material nodes in the numerical model were constrained to accurately replicate the effect of HBP in pure epoxy resin, and a Monte Carlo method was used to simulate the random distribution of HBP. The numerical model was validated by fracture tests with single-edge-notched bending (SENB) samples. Moreover, the effect of the HBP weight fraction on the fracture properties was analysed. With increasing HBP weight fraction, a three-stage increase of mode-I fracture toughness in a rapid-slow-rapid manner was obtained. Overall, the proposed modified peridynamic method provided a macroscale analysis of the fracture behaviour of nanocomposites reinforced by HBP in a simulation framework.

Keywords: nanoparticles, reinforced fracture behaviour, Monte Carlo simulation, SENB fracture samples

1. Introduction

Epoxy resin, used as a matrix of composite materials, has received great attention due to its wide application in the aerospace industry as it allows to enhance the lightweight and anti-corrosion features of composite materials. However, epoxy resin is also the possible weak point of composite materials, considering its mechanical features, i.e., low strength, poor fracture resistance and brittleness. It behaves as the dominant damage location inside composites under some in-service loading conditions like impact [1] and fatigue [2]. As a result, improving the fracture resistance of epoxy resin is important, and adding particle materials is one of the promising solutions [3]. According to existing investigations, introducing polylactide [4], graphene oxides [5], nanoparticles [6] and hyperbranched polyester (HBP) [7] to epoxy resin can greatly increase its fracture toughness. In particular, neat epoxy or composites, which contain HBP, show not only outstanding fracture properties [7,8] but also excellent thermal

properties along with an increased glass transition temperature. Additionally, HBP particles are also a low-cost option for industrial applications.

According to the work of Verrey *et al.* [9], by introducing HBP to the matrix of carbon-fibre-reinforced polymer (CFRP), double cantilever beam tests presented a higher mode-I fracture toughness compared with neat epoxy. In addition, mode-II fracture toughness can also be improved by adding HBP to the matrix due to the interaction between the epoxy resin and the HBP particles [10], where a perfect interphase can be witnessed between both components [11]. In order to further investigate the effect of HBP on the matrix of composites, attention should focus on the structure and properties of the pure resin with HBP particles [7,8,12]. It has been reported that HBP increases the fracture toughness of epoxy by 60–90% with a HBP weight fraction of 1–5 wt.% [7]. Such an improvement is also affected by the type of HBP and the chemical functions carried by the particles [8]. More so, potential enhancements on the neat epoxy could also be achieved by mixing HBP with other nanoparticles [13,14].

Considering the cost of experimental activities and the various factors (e.g., chemical functions, weight fraction, etc.) that can affect the strengthening effect of HBP on the epoxy resin, the development of virtual tests to investigate the fracture properties is of great interest. For neat resin, numerical methods are capable to provide reliable results of the quasi-static fracture tests for both compact-tension (CT) [15] and single-edge-notched bending (SENB) [16] specimens. Nevertheless, it is easier to conduct such investigations on neat and typical composite materials than on nanocomposites. The effect of nanoparticles like HBP, even under simple loading configurations, including flexure [10] and tension [12], leads to the limitation of applying related mechanical properties in fracture simulations, unlike the neat material [17]. Furthermore, due to the complex geometries and uncertainty distributions of HBP, the modelling process remains challenging and, thus, limited numerical simulations are presented in existing studies. However, as far as the interface is concerned, a perfect bond between the HBP and epoxy can be assumed in the model [18], and the small size of the HBP allows for the simplification of numerical modelling [19].

Generally, replicating the fracture behaviour in a classical numerical environment is not straightforward, especially the replication of the random crack path and the generated free surfaces. With the recent developments in computational mechanics, new methods have been proposed to address the aforementioned numerical issues in fracture simulations. For instance, extended finite element modelling is able to produce a crack path in any position of the numerical model without being limited by the mesh morphology; however, the analysis requires many parameters [20]. In addition, atomistic molecular dynamics (MD) simulation is one of the competitive techniques [21], which builds the model based on the molecular structures and bonds between them. MD simulations can endow the free surface energy on a molecular scale, and the breaking of the bonds can introduce more freedom for the crack path. However, most of the studies employing MD simulations consider unit cells under simple loading

conditions instead of fracture of a real component [22]. This choice can mainly be attributed to the time-consuming calculations, which hinder its application to large structures, including SENB specimens. Compared with MD simulations, the cutting-edge method proposed by Silling [23], which employs a peridynamic model, is a better choice to model the fracture behaviour of structures. The peridynamic theory is based on integral-differential equations. The governing equations are always valid, regardless of whether or not there is any discontinuity in the structure. The method is further based on basic equations of motion and forces (in Greek, 'peri' means 'horizon' and 'dynamics' means 'force'). Therefore, it can mimic random cracks, and the mechanical behaviour, by setting bonds between elements, which helps to easily generate free fracture surfaces. It is capable of providing reliable results with only a limited number of required parameters [24,25], especially for linear-elastic/brittle materials [26]. Additionally, the peridynamic method has been modified frequently to replicate the mechanical behaviour of nanocomposites due to its inherent non-local features [27,28]. However, for these materials, an enhanced material model development and a reconstructed stress calculation are required based on a strong mathematical basis.

In the present work, a phenomenological modified peridynamic method is proposed to mimic the fracture behaviour of nanocomposites reinforced with nanoparticles. The objective of the present work is to check the capability of the proposed method to capture experimental data [29] from fracture tests [7,8] using SENB samples of HBP-reinforced epoxy resin. The proposed method uses peridynamics to simulate the fracture behaviour with randomly constrained nodes mimicking the effect of HBP particles. Additionally, the Monte Carlo method has been employed to achieve the random distributions of the HBP particles. In comparison with a typical modelling methodology on nanocomposites, the proposed modified peridynamic method is not only able to characterise the behaviour of nanocomposites at a macroscale, but it also greatly simplifies the modelling process.

2. Modelling methodology

2.1 Background of the peridynamic method

Unlike typical mechanical methods employing spatial differential terms to present deformation, the peridynamic method uses non-local nodal integral terms to build the load transformation among the material points, which are the basic elements for the peridynamic method. Actually, peridynamics can be regarded as an update of MD simulation at a macroscale, which does not consider too many parameters of the microstructures [28] and which is also suitable for the non-local replication of discontinuous fracture behaviour. The latter is difficult to address in a typical mechanical numerical framework.

In the peridynamic environment, mainly two methods are used to reproduce the connection among neighbouring material points: bond-based [23] and state-based [30] methods. The bond-based peridynamic method typically uses bonds to link a material point with its neighbouring point, and the

stretching, and breaking of the bonds describe the deformation and failure of the material. As reported in [31], the bond-based peridynamic method is able to capture the tensile behaviour by the stretching of bonds, but it cannot be applied to compressive loading. Additionally, due to the sudden breaking of bonds without stiffness degradation, bond-based peridynamics are only employed for the simulation of the failure of brittle materials. State-based peridynamics on the other hand describes materials with the energy absorbed among material points and are designed to address the aforementioned problems, i.e., without being limited to the tensile behaviour of brittle materials. Through the use of an energy-updating process, state-based peridynamics can be applied to both plastic behaviour [32] and damage behaviour under various loading conditions [33].

In the present work, peridynamics was utilised to mimic the fracture tests of SENB specimens on HBP/RTM-6 nanocomposites. Based on existing material tests [7], the constitutional behaviour of nanocomposites can be regarded as linear with a sudden failure. Furthermore, only a mode-I fracture is involved in the fracture tests, which is an open-mode fracture behaviour, purely determined by the tensile behaviour of the material [16]. As a result, bond-based peridynamics was used, more specifically the method implemented in the commercial finite element modelling (FEM) software LS-DYNA. More details about the peridynamic method in LS-DYNA can be found in Section 2.2, while the capability of this method was proven by the validation on neat resin in Section 3.1.

2.2 Brief review of the peridynamic method in LS-DYNA

Bond-based peridynamics in LS-DYNA is achieved by the weak-form discontinuous Galerkin method. According to the peridynamic theory, the equation of motion for any point (\mathbf{X}) at a specific time point t can be presented as:

$$\rho \ddot{\mathbf{u}} = \sum_{H_{\mathbf{X}}} \mathbf{f}(\mathbf{u}(\mathbf{X}',t) - \mathbf{u}(\mathbf{X},t), (\mathbf{X}' - \mathbf{X})) dV_{\mathbf{X}'} + \mathbf{b}(\mathbf{X},t) \quad \text{Eq. (1)}$$

where $H_{\mathbf{X}}$ is the horizon, effective region, of point \mathbf{X} , \mathbf{b} is the body force density and ρ is the mass density of the objective. Additionally, \mathbf{f} represents the force function of the interaction between point \mathbf{X}' and \mathbf{X} , whose displacement vector field can be expressed by \mathbf{u} .

Following the Galerkin weak form adopted in LS-DYNA, Equation (1) can be written as:

$$\int_{\Omega} \rho \ddot{\mathbf{u}}(\mathbf{X}) \cdot \mathbf{v}(\mathbf{X}) dV_{\mathbf{X}} = \int_{\Omega} \int_{H_{\mathbf{X}}} \mathbf{f}(\mathbf{u}(\mathbf{X}',t) - \mathbf{u}(\mathbf{X},t), (\mathbf{X}' - \mathbf{X})) dV_{\mathbf{X}'} \cdot \mathbf{v}(\mathbf{X}) dV_{\mathbf{X}} + \int_{\Omega} \mathbf{b}(\mathbf{X}) \cdot \mathbf{v}(\mathbf{X}) dV_{\mathbf{X}} \quad \text{Eq. (2)}$$

$$\forall \mathbf{u}(\mathbf{X}) \in S(\Omega), \mathbf{v}(\mathbf{X}) \in S'(\Omega)$$

where Ω is the computational domain, $S(\Omega)$ is the solution located in a subspace of Banach space, expressed as $S(\Omega) = \{\mathbf{u}(\mathbf{X}) \in L^2(\Omega) \mid \mathbf{u}(\mathbf{X}_g) = g(\mathbf{X}_g) \forall \mathbf{X}_g \in S_B\}$ where S_B is the boundary, and $S'(\Omega)$ is the space in which the test function $\mathbf{v}(\mathbf{X})$ is located. Then, the approximation field for the test function

is constructed based on the shape function of the regular FEM as: $u_i(\mathbf{X}) = u_i^A N^A(\mathbf{X})$, $v_i(\mathbf{X}) = v_i^A N^A(\mathbf{X})$, where u_i^A represents the nodal displacement u_i of node A. Thus, the first-level integration of Equation (2) can be expressed as:

$$\sum_{g=1}^{n_g} \rho N^B(\mathbf{X}^g) \Delta V^g \ddot{u}_i^B = \sum_{g=1}^{n_g} \left(\int_{H_{\mathbf{X}'}} f_i(\boldsymbol{\eta}(\mathbf{X}^g), \boldsymbol{\xi}(\mathbf{X}^g)) dV_{\mathbf{X}'} \right) \cdot N^B(\mathbf{X}^g) \Delta V^g + \sum_{g=1}^{n_g} b_i(\mathbf{X}) N^B(\mathbf{X}^g) \Delta V^g \quad \text{Eq. (3)}$$

Herein, n_g denotes the total number of Gaussian points in the calculation region with $\boldsymbol{\eta} = \mathbf{u}(\mathbf{X}', t) - \mathbf{u}(\mathbf{X}, t)$ and $\boldsymbol{\xi} = (\mathbf{X}' - \mathbf{X})$. Based on the calculation conducted on related Gaussian points in Equation (3), the bond connection can be defined to represent $\boldsymbol{\eta}$ and $\boldsymbol{\xi}$ as:

$$\begin{cases} \boldsymbol{\eta}(\mathbf{X}^g) = N^A(\mathbf{X}^g) \mathbf{u}^A - N^{A'}(\mathbf{X}^{g'}) \mathbf{u}^{A'} \\ \boldsymbol{\xi}(\mathbf{X}^g) = N^A(\mathbf{X}^g) \mathbf{X}^A - N^{A'}(\mathbf{X}^{g'}) \mathbf{X}^{A'} \end{cases} \quad \text{Eq. (4)}$$

Considering all the above-mentioned processes, the bond-based explicit peridynamic method governing equation can finally be obtained as:

$$\sum_{g=1}^{n_g} \rho N^B(\mathbf{X}^g) \Delta V^g \ddot{u}_i^B = \sum_{g=1}^{n_g} \left(\sum_{g'=1}^{n_{g'}} f_i(\boldsymbol{\eta}(\mathbf{X}^g, \mathbf{X}^{g'}), \boldsymbol{\xi}(\mathbf{X}^g, \mathbf{X}^{g'})) \Delta V^{g'} \right) \cdot N^B(\mathbf{X}^g) \Delta V^g + \sum_{g=1}^{n_g} b_i(\mathbf{X}^g) N^B(\mathbf{X}^g) \Delta V^g \quad \text{Eq. (5)}$$

where $n_{g'}$ is the number of all neighbouring points of \mathbf{X}^g ; B loops to cover all Gaussian points in the domain. The calculation based on the peridynamic method can then be carried out.

As the approximation is carried out based on the regular FEM shape function, detached FEM elements are employed in the calculation, and Gaussian points within each element are regarded as calculation units for the peridynamic method. As a result, a boundary enforcement can be directly applied in the same way of the FEM method, which can avoid the boundary issues of a typical non-local method. The same peridynamic method implemented into LS-DYNA has been used in the works of Ren, *et al.* [24] and Mehrmashhadi, *et al.* [34], which can be regarded as a validation of the method.

In bond-based peridynamics, the definition of the properties of the bonds among the material points is of great importance as it determines the material behaviour, whereas, in classical mechanical methods, the focus lies on the elastic modulus and strength. Therefore, in the present study, the microelastic modulus (c) and the critical bond stretch (s_c) are used to describe the bond properties, which are hard to obtain from experiments [24]. However, the prototype microelastic brittle (PMB) material model [35] can help to calculate both values, where the bonds are regarded as springs in a linear-elastic material. Herein, the force of a bond under loading (f) can be presented by its stored elastic energy (w), which is called micropotential in the PMB model, with the relative displacement of

the material point (d) and the length of the bond (l) considered. Accordingly, the formula of f is shown below:

$$f(d,l) = \partial w(d,l)/\partial d \quad \text{Eq. (6)}$$

Since the bond is regarded as a spring, the energy absorbed, or the micropotential, can be obtained based on Hooke's law from:

$$w(|d|,|l|) = \frac{1}{2}cs^2|l| \quad \text{Eq. (7)}$$

where $s = \frac{|d+l|-|l|}{|l|}$ is the bond-stretch ratio. As a result, the tensile load on the bond under tension can be derived with a constant c for the existing material by:

$$f(d,l) = cs \quad \text{Eq. (8)}$$

Furthermore, the effect of one material point can be described by a sphere with a radius (δ) instead of just being linked with its closest material points. So, $f(d,l) = 0, \forall |l| > \delta$. The assumption of this sphere, or the parameter δ , also known as the normalised horizon size in the numerical environment, makes the peridynamic method non-local. Moreover, failure of the bond, judged by the energy release rate (G_c) can be presented in a 3D geometry with the critical length of bond (s_c) through [24]:

$$G_c = \frac{\pi cs_c^2 \delta^5}{10} \quad \text{Eq. (9)}$$

The information presented above forms the basis of bond-based peridynamics in terms of the loading and failure processes. However, other algorithms are also involved to achieve a stable calculation, such as the application of the Galerkin weak form for boundaries and the approximation as FEM method for the shape function. More details can be found in [24]. Another key challenge is to link the parameters involved in peridynamics with those obtained at the macroscale. By bridging the two scales using:

$$3E = \sum \frac{1}{12}c|\varepsilon|\Delta V' \quad \text{Eq. (10)}$$

$$s_c = \frac{1}{\delta^2} \sqrt{\frac{10G_c}{\pi c \delta}} \quad \text{Eq. (11)}$$

the microelastic modulus (c) and the critical bond stretch (s_c) can be calculated. Indeed, the relationship between the microelastic modulus and the macroscale elastic modulus (E) is given by Equation (10), where $\Delta V'$ is the related volume difference due to the deformation and rigid movement of the central material point. Equation (10) is proposed with the elastic energy collection on the material points, in which the elastic energy density of a Gaussian point (a unit region) in the macroscale is equal to the energy density absorbed by all the bonds in this unit region within the peridynamic method. Compared

with the typical equation $c = \frac{18\kappa}{\pi\delta^4}$, used to build such relationship, Equation (10) employed in the current work can fix the calculation issues found near the boundary and for non-uniform deformation [24]. Equation (11) is derived from Equation (9) and can be used to obtain the critical bond stretch (s_c) from the energy release rate (G_c) and the microelastic modulus (c). As a result, the peridynamic method can be applied to simulate the mechanical response of linear-elastic/brittle materials under tension. The elastic modulus and the energy release rate determine the mechanical response and failure process, with the failure of the material initiating between each element.

2.3 Assumptions and the method to mimic the effect of nanoparticles

HBP particles are generally used to enhance the fracture toughness of resin materials. The particles' geometrical structure is complex due to the existence of branches [19]. However, due to the presence of the branches, the bonds between the HBP particles and resin are generally supposed to act as a perfect bond [11]. Usually, nanocomposites with HBP particles are regarded as isotropic materials. However, such nanocomposites can be locally anisotropic, depending on the manufacturing process, and this behaviour can be considered in modelling approaches at a small scale. More details about the HBP particles employed in the present work can be found in [7].

The peridynamics method performs outstandingly in case of rapid failure and, thus, the onset of discontinuity inside materials, provided that it is applicable. Indeed, bond-based peridynamics is developed for isotropic materials due to the use of the PMB material model. A possible local anisotropy in nanocomposites cannot be described by the PMB model and consequently hinders the direct application of bond-based peridynamics. In order to apply peridynamics on nanocomposites, modifications were introduced at the microscale [28] and multiscale [27], and were combined with other methods, such as MD [36] or uncertainty distributions [37]. For nanocomposites, all these modifications are necessary, though they require a strong mathematical and programming basis.

For the HBP/RTM-6 nanocomposites of the present work, the complex geometry of HBP, especially its branches in the microstructure, hinders a very detailed modelling process. The interface between the HBP and epoxy resin, on the contrary, was found to be perfect [11]. The perfect interface can be easily captured by a permanent tie or constrained entities in the present numerical framework. Additionally, the influential region of HBP is always small inside the epoxy resin and, specifically, the radius of the sphere region affected by one HBP particle is $\sim 15 \text{ \AA}$, according to MD simulation [19]. If modelled at an angstrom-scale/nanoscale, the complicated geometry of HBP cannot be ignored. However, with the increase of the modelling scale from nanometre to micrometre or millimetre, as shown in Figure 1, the complex geometry of HBP's branches can be ignored because the nanoparticles are concentrated in the centre. HBP particles are thus perfectly incorporated into epoxy resin. From the modelling perspective, these features of HBP particles can therefore be considered as the constraints of material points in the matrix. As a result, it could be feasible to capture the effect of the HBP through

constraining the nodes of detached elements in the framework of the peridynamic method in LS-DYNA. Additionally, considering that the weight fraction of HBP particles is relatively low (<10 wt.%), the case of more than one HBP particle concentrated with another particle in a local region is highly unlikely and, thus, this situation was not considered in the analysis. Compared with existing modified methodologies on peridynamics for nanocomposites [27,28], the present modification can be regarded as a phenomenological one because it can be performed by updating the geometrical mode rather than the core algorithm of peridynamics.

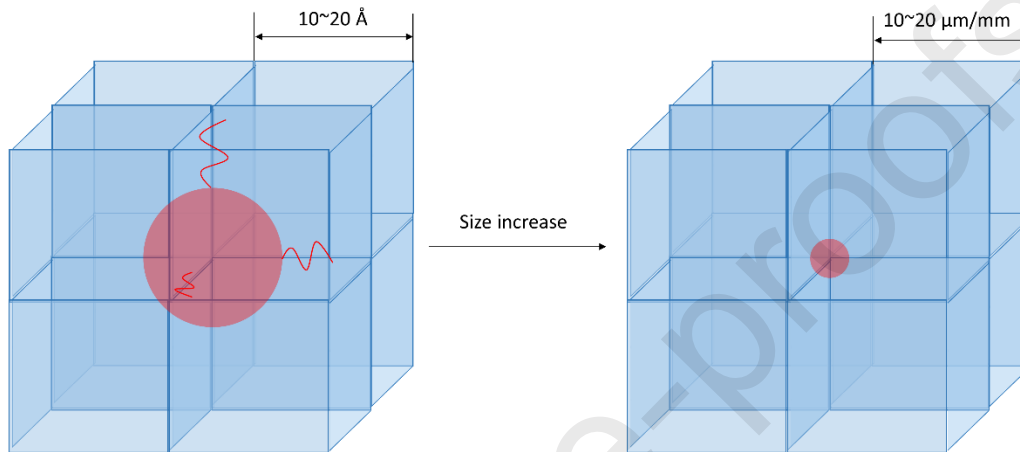


Figure 1 Simplification of the hyperbranched polyester (HBP) geometry resulting from an increase of the scale

2.3 Finite element model

The geometry implemented in the finite element model for the SENB fracture tests considered in the present work is presented in Figure 2. The model was built based on an experimental setup according to [7,8,29]. The sample has a thickness of 3 mm. The model consists of three different parts: peridynamic elements in the centre near the crack tip, assigned by ELFORM=48 in LS-DYNA (see blue part in Figure 2), constant stress solid elements (see brown part in Figure 2) and rigid bodies to mimic the loading and support parts (see grey part in Figure 2). While in the real samples, in line with the ASTM D5045 standard [38], the length of the notch before the test varied from 0.45 to 0.55 times the height of the sample (6 mm), a fixed length of 3 mm was chosen in the numerical model to reduce the modelling complexity. In order to improve the calculation efficiency, not the entire sample was built through peridynamics but only the part which determines the fracture behaviour in such tests, i.e., the material adjacent to the crack tip. The remaining part of the sample was modelled by constant stress solid elements with a rough mesh to provide an acceptable geometry/deformation but with a reduced computational cost. In order to ensure a smooth stress transfer, the contact between the peridynamic and solid elements was modelled by `Constrained_FEM_PERI_Tie`. With the boundary condition constrained in such a way, the information related to stress/force and deformation can be transferred between the FEM and peridynamic parts in the form of an all-constrained boundary condition. Figure 3 shows the stress continuity from the peridynamic elements to solid elements close to two critical

positions, i.e., the loading point and crack tip. In Figure 3, state #1 represents the state at the onset of the fracture. State #2 is the state when the stress reaches the boundaries between solid elements and peridynamic elements, which validates the constrained boundaries. It should be noted that a better performance can be achieved with the same mesh size of the peridynamic and solid parts on their boundaries (as shown in Figure 3).

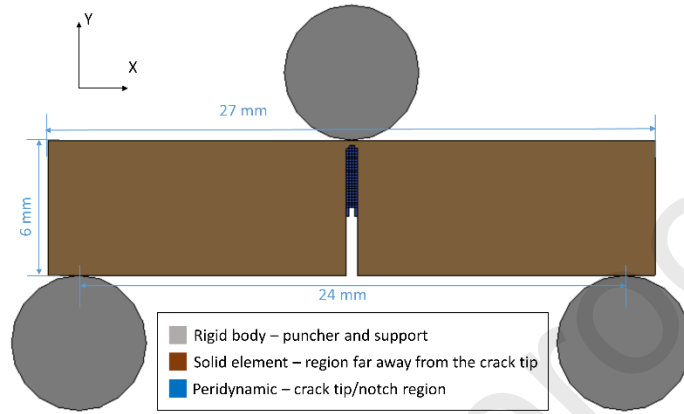


Figure 2 Schematic presentation of sample and boundary conditions implemented in the finite element model for the single-edge-notched bending (SENB) fracture tests simulation (front view)

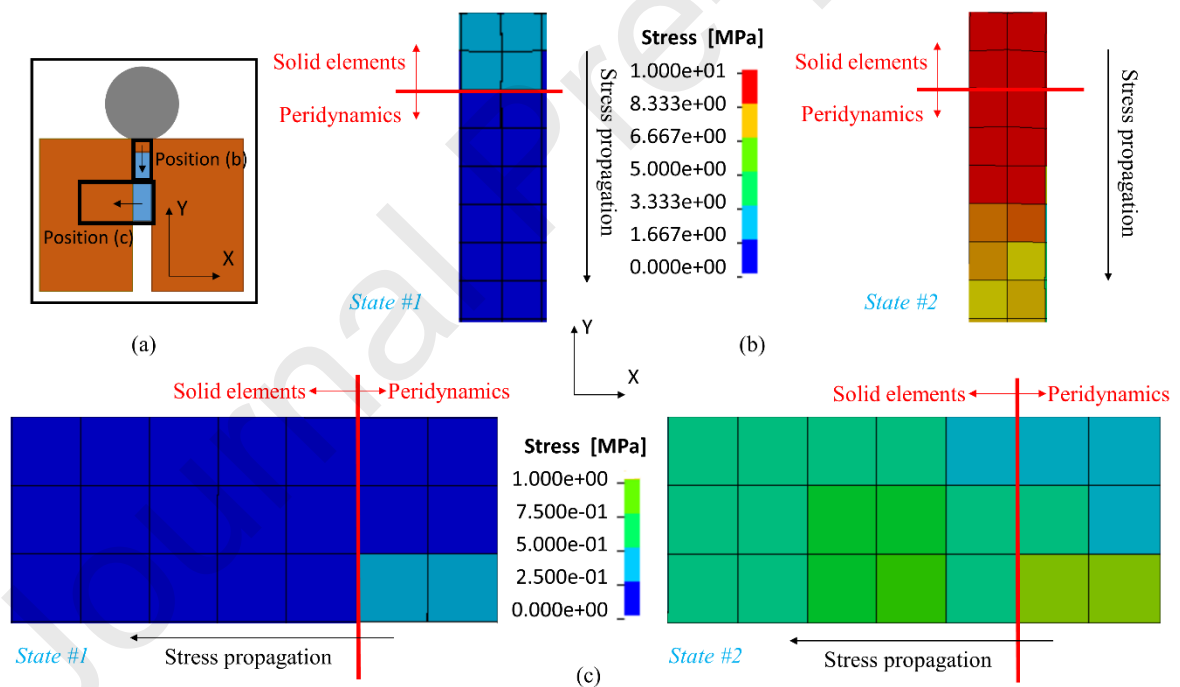


Figure 3 von Mises stress continuity at the crack tip (b) and near the puncher (c) at the constrained boundary between solid and peridynamic elements with a more accurate location (a). State #1 is at the initiation of the crack, and state #2 is the stress reaching the boundary of the peridynamic and solid elements.

During loading in the tests, no deformation of the puncher and supports occurred, and consequently, they were set as rigid bodies. Regarding the boundary conditions, the supports were fixed, and the puncher was allowed to move in the loading direction. The loading process was replicated through the displacement of the puncher with a constant velocity, while the total kinetic energy was

kept below 10% of the total energy to guarantee quasi-static loading conditions. Additionally, automatic surface-to-surface contact was employed with no friction between the sample and the puncher/supports.

Considering the material, the elastic models Mat_Elastic_Perid (Mat_000) and Mat_Elastic (Mat_001) were employed for the peridynamic part and solid part of the sample, respectively. Since the density of the material is practically not affected by the addition of nanoparticles [17], a density of 1440 kg/m³, i.e., the density of pure matrix (RTM-6), was used for all sample materials. For the elastic modulus, the experimental values listed in Table 1 were used for the material with different weight fractions of the HBP particles [7]. The failure of the material was determined by the mode-I energy release rate (G_{IC}), which is equal to 0.113 kJ/m² for neat epoxy resin, according to fracture tests with SENB specimens [7,8]. The Mat_Rigid (Mat_021) model was assigned to the rigid supports and puncher.

Table 1 Elastic modulus with different weight fractions of hyperbranched polyester (HBP) particles [7]

Properties	Parameters			
Weight fraction (wt.%)	0.0 (neat)	0.1	1.0	5.0
Elastic modulus (MPa)	2558	3300	2992	2980

In view that the results of fracture tests are mainly determined by the material properties near the crack tip, the method using constrained nodes to replicate the effect of HBP particles was only introduced to the peridynamic region. Considering the perfect interface with the matrix and the limited influential region, the HBP particle was not directly created in the numerical model. Instead, all nodes sharing the same location with the corresponding HBP particle were constrained to mimic the presence of HBP particles in the matrix. Based on the hypothesis that the HBP particles and epoxy resin have a similar density, the number of constrained nodes was calculated from the total number of nodes in the neat epoxy model and the weight fraction of the nanoparticles, according to Equation (12). In all cases for nanocomposites, the energy release rate was 0.113 kJ/m², the same as the neat epoxy resin rate. This choice was made with the aim to check if the output of the stress intensity factor and energy release rate can be captured through partially constrained nodes in the model as proposed in the present work. For instance, there are 1400 nodes in the peridynamic part of the model with the mesh size of 0.12 mm. As a result, the number of constrained nodes for 1.0 wt.% nanocomposite case should be equal to 14, i.e., $1400 \times 1.0\%$.

$$N_{constrained} = N_{total} \times wt.\% \quad \text{Eq. (12)}$$

2.4 Monte Carlo method

Following the determination of the number of constrained nodes according to the weight fractions, the distribution/position of these nodes for the replication of the HBP particles should be analysed further. Considering that the real distribution of nanoparticles inside the epoxy resin is locally random, an arbitrary distribution was employed in the numerical model as shown in Figure 4. The

process to automatically achieve the Monte Carlo simulation is briefly introduced here. Firstly, the node information at each possible location was collected in a set. During the modelling, some sets were selected and constrained according to the amount determined by Equation (12). In this way, the Monte Carlo simulation was able to start in the present work to consider the effect of the different distributions. Herein, all potential sets were built through Matlab, while the automatic process of the Monte Carlo simulations was conducted in LS-OPT, and the calculation was made through the explicit solver of LS-DYNA. In order to obtain a reliable result and cover sufficient cases, at least 50 Monte Carlo simulations were used for each weight fraction. Moreover, the scatter of the fracture toughness observed in the experimental activities was also compared to the simulated range, which was determined by the HBP distributions. Overall, the constrained nodes can represent the effect of nanoparticles, while the peridynamic method works on the resin without modification to achieve the local anisotropy. Compared with a typical modification of the peridynamics for nanocomposites, the present method is more simplified because the consideration of nanoparticles is achieved on a geometrical instead of a theoretical level. The constrained nodes can represent the effect of nanoparticles, while the peridynamics method works on the resin without modification to achieve the local anisotropy.

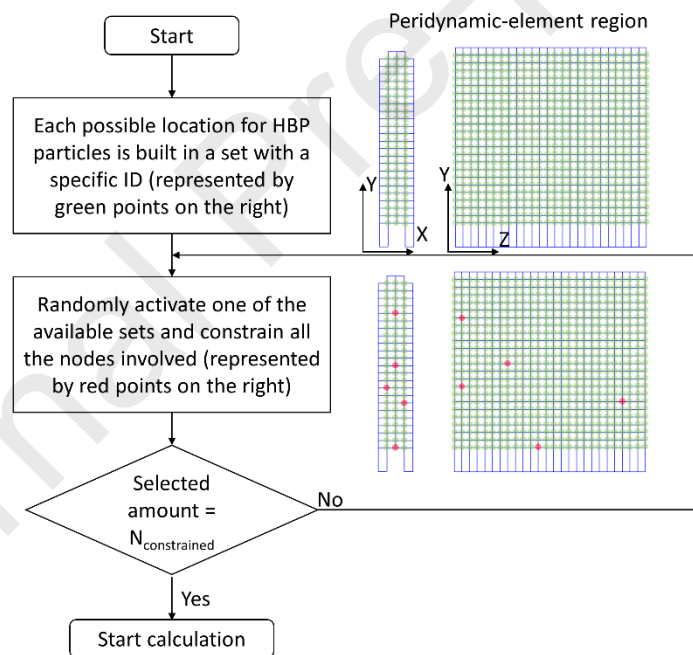


Figure 4 Schematic presentation of the generation of the random distribution of hyperbranched polyester (HBP) particles

2.5 Mesh size sensitivity

Although the peridynamics method has been originally proposed as a meshfree method, the peridynamic element implemented in LS-DYNA is transformed from a normal FEM element. As a result, it is also necessary to discuss the effect of the mesh size in the present work. Herein, the stress intensity factor (SIF, K_{IC}) and energy release rate (G_{IC}) were considered in the investigation of the mesh size effect in the simulations of fracture tests. Figure 5(a) presents the mesh size sensitivity of the results

obtained for neat resin. Both K_{IC} and G_{IC} started to converge when the size was smaller than 0.12 mm with a calculation time of 33 min for the 0.12 mm mesh and 6 hours for the 0.06 mm mesh with 6 CPUs (I7–875K 2.93GHz 4 core/8 threads – 16 GB RAM). Therefore, the 0.12 mm mesh was chosen for the present work.

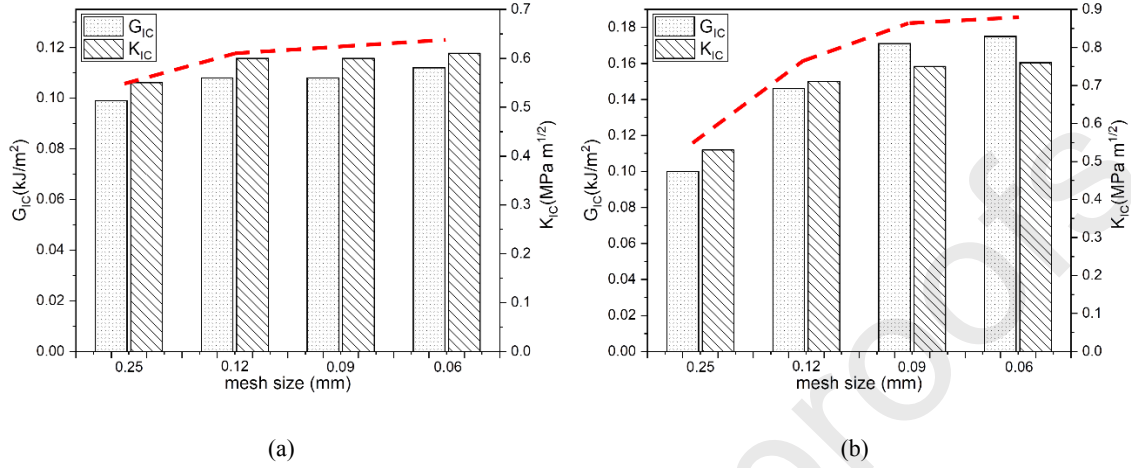


Figure 5 Mesh size sensitivity analysis for neat resin (a) and 1.0 wt.% nanocomposite (b) with the red dashed lines presenting rough trends of the parameters

However, the mesh size sensitivity study on the neat case may not be sufficient for the present work considering the involved constrained nodes. Indeed, the mesh size determines the total number of nodes in the numerical model of the nanocomposites, which affects the number of constrained nodes according to Equation (12). As a result, the effect of the mesh size for the nanocomposite simulations is potentially different from the neat epoxy case. Taking 1.0 wt.% HBP as an example, the results become stable at a mesh size of 0.09 mm as opposed to a value of 0.12 mm for neat epoxy, as can be seen from the red dashed lines in Figure 5.

Since the mesh size required to reach convergence is clearly affected by the fraction of nanoparticles, three different mesh sizes, i.e., 0.12, 0.09 and 0.06 mm, were considered in the following analyses. However, for the finest-mesh-size model, the Monte Carlo simulation took 300 hours (6 hours/case \times 50 cases). Therefore, attention should be paid to the minimum mesh size required when the proposed method is applied, especially if different weight fractions are considered. In section 3, the simulation outcome is compared with experimental data.

3. Results and discussion

3.1 Validation for the neat epoxy

Prior to the application on nanocomposites, the numerical model and the related parameters were validated for the neat case. Figure 6 presents the results from the numerical model and its comparison with experimental data. The formation of a centre crack from the notch can be witnessed in the red-marked region presenting the failure location from the numerical model (see Figure 6(a)), owing to the breaking of the bonds among the elements at the crack tip. Additionally, a crack map (see

Figure 6(b)) was created with the focus on the peridynamic part, i.e., the main cracking part of the numerical model, which clearly shows the crack propagation.

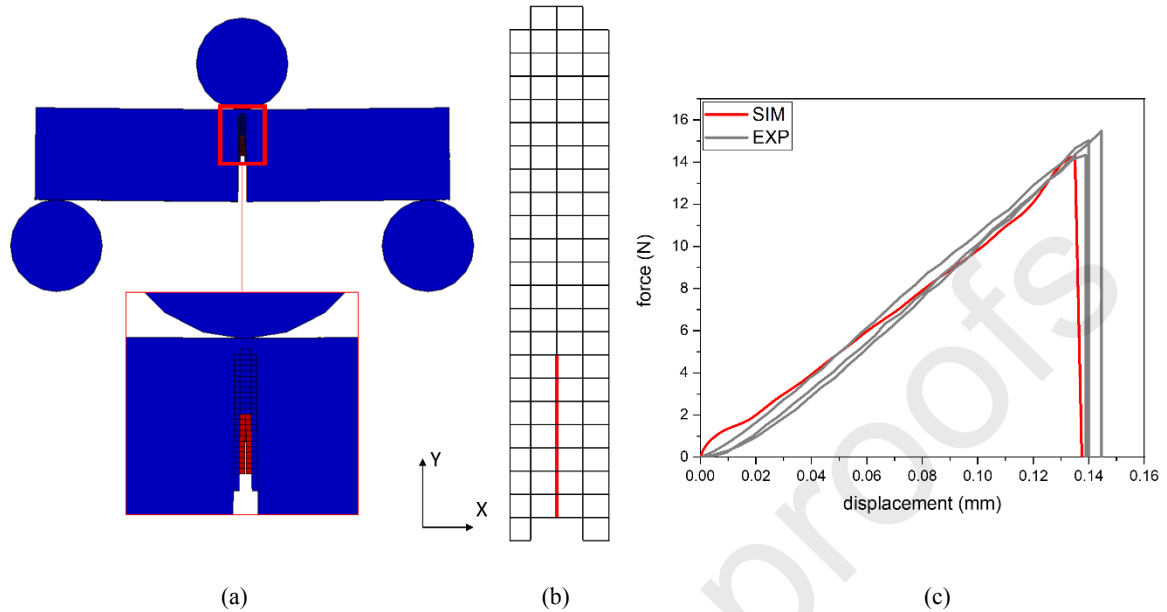


Figure 6 The crack propagation (a) and crack path (b) from the numerical model, and comparison between experimental [29] and simulated force-displacement curves (c)

As is clearly visible in Figure 6(c), a good agreement was obtained between the force-displacement curves from the numerical model and the experiments [29]. Additionally, the modelled SIF and G_{IC} were also close to the experimental results: $0.6MPa \cdot m^{1/2}$ and $0.108kJ/m^2$ from the numerical model compared with $0.62 \pm 0.06MPa \cdot m^{1/2}$ and $0.113 \pm 0.01kJ/m^2$ from the tests [7]. According to the ASTM standard on fracture tests [38], the SIF is determined by the peak force while G_{IC} is calculated by both the peak force and the displacement at the peak, meaning that the force-displacement curves are reflected in the SIF and G_{IC} values. Unlike the force-displacement curves, which are significantly affected by the notch size when calculating the SIF and G_{IC} , calibration factors can be used, which drastically reduce the effect of the samples' notch geometry [16]. As a result, in the next sections, the SIF and G_{IC} were used to validate the results instead of the force-displacement curves.

3.2 Simulation results of nanocomposites

The SIF and G_{IC} results from the numerical models and experiments are reported in Figure 7 for the different weight fractions considered. While a single set of values was obtained for the neat resin, for the nanocomposite cases, several values were obtained for the fracture parameters, as the Monte Carlo approach was used for the particle distributions. The curves obtained from the models are reported in Figure 7, showing both average values (identified by the lines) together with the obtained range. Again, a good agreement between test and modelling results was obtained. The fracture properties were significantly improved when the HBP fraction increased from 0 to 0.1 wt.% and from 1.0 to 5.0 wt.%, while a tiny increment was present when the weight fraction changed from 0.1 to 1.0

wt.%. However, the trend was similar for both the numerical model and experimental data. Figure 7 also contains the numerical results using the three different mesh sizes. Both SIF and G_{IC} converged and approached the experimental data when the mesh size was reduced. However, the mesh size needed for convergence depended on the weight fractions: 0.12 mm for 5.0 wt.%, 0.09 mm for 1.0 wt.% and 0.06 mm for 0.1 wt.%. This led to the important conclusion that the present model more easily reached convergence for nanocomposites with a higher weight fraction of HBP. Additionally, for all the results presented in Figure 7, the scatter increased with the particle weight fraction. This phenomenon is attributed to the fact that a variety of distribution patterns exists for nanoparticles inside the epoxy resin and that the possible number of cases assigning a certain number of tied nodes to the model increased with the weight fraction.

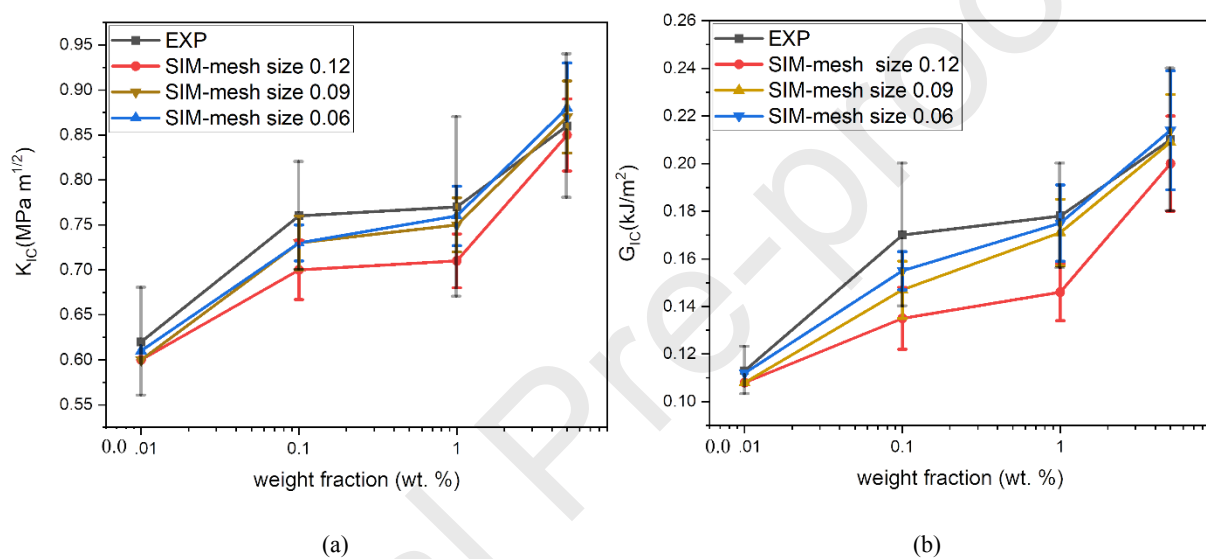


Figure 7 Comparison of stress intensity factor (SIF) (a) and G_{IC} (b) obtained from the numerical models with various mesh sizes and experimental data for different hyperbranched polyester (HBP) weight fractions

3.3 Effect of hyperbranched polyester (HBP) on fracture behaviours of nanocomposites

According to Figure 7, both numerical and experimental curves reported the same three-stage trend for the fracture properties: a rapid-slow-rapid increase as the weight fraction increased from 0 to 5.0 wt.%. In order to explore which physical mechanism contributes to this phenomenon, an additional investigation into the numerical framework was conducted using the model with a mesh size of 0.12 mm to reduce the calculation time.

Firstly, the relationship between the HBP distribution and crack propagation path was studied. As visible in Figure 8, four special cases, i.e., D1, D2, D3 and D4, of the HBP distributed within the cracking region (see blue part in Figure 2) are presented: D1 and D4 gather the constrained nodes at the notch tip, while D2 and D3 spread the constrained nodes from the notch tip to the interior. Here, the blue dots mark the constrained location, and the red arrows show the paths of the crack propagation, according to the simulation results. The total number of constrained nodes was identical in all four cases, based on the nanocomposite with a weight fraction of 1.0 wt.%, but a specific condition of

gathering all the constrained nodes near the notch tip was adopted. The comparison of D1, D2 and D3 leads to a substantial improvement of the SIF when the constrained nodes gather near the notch tip, while the constrained nodes located far from the notch tip have practically no effect on the SIF. This enhancement was caused by the fracture behaviour in the SENB tests, which was mainly dependent on the material behaviour at the notch tip, as the reinforcement of HBP can improve the SIF efficiently when located near the notch tip. The reinforcement of the constrained nodes for case D4, for which the constrained nodes are located close to the external boundary of the peridynamic region, was larger compared with D1, for which the constrained nodes are located around the centre (see blue part in Figure 2). This can be attributed to the fact that the exterior surface is in a plane-stress state, while the centre of the sample can be regarded as a plane-strain state, and the reinforcement of nanoparticles on the fracture properties is more significant in the plane-stress state than in the plane-strain state, according to the fracture mechanism [39].

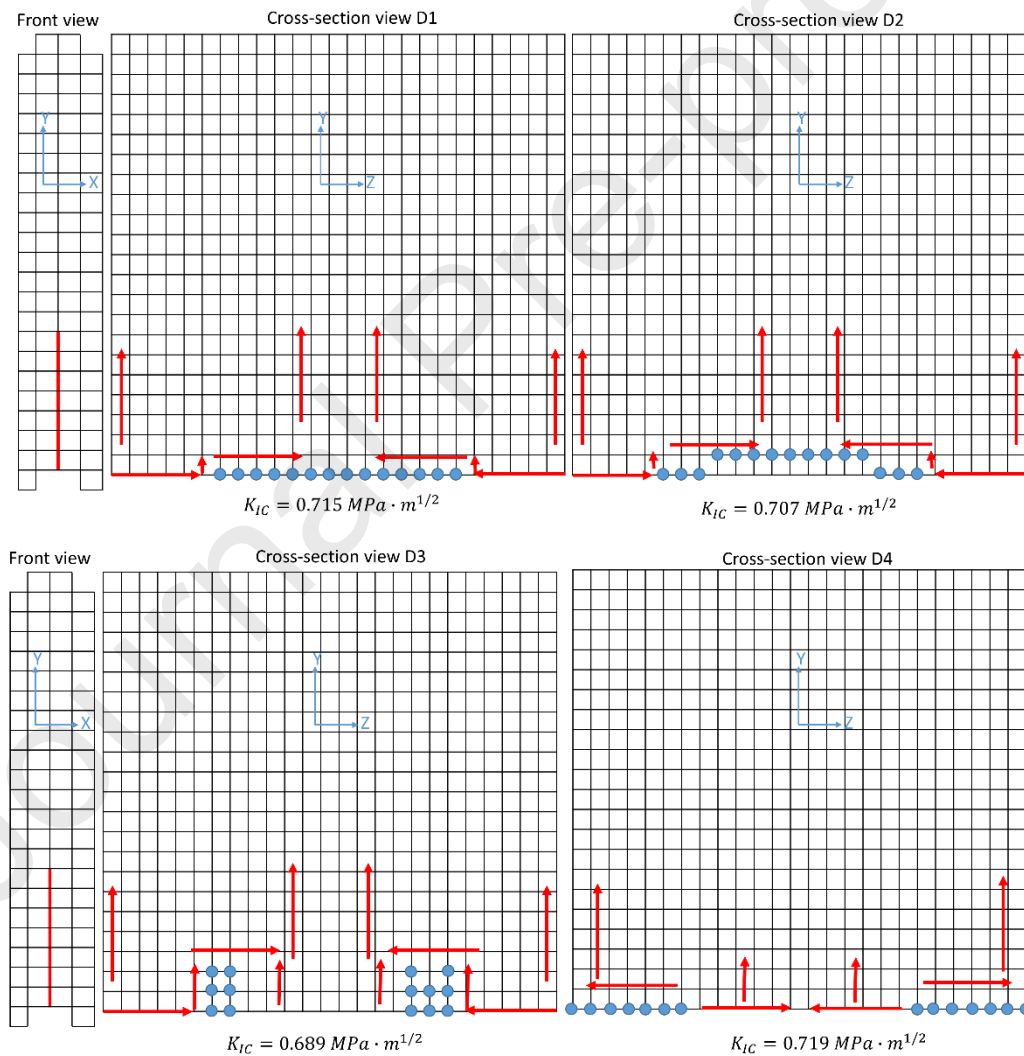


Figure 8 Four cases representing the effect of different hyperbranched polyester (HBP) distributions on the simulated crack. The red arrows present the crack propagation.

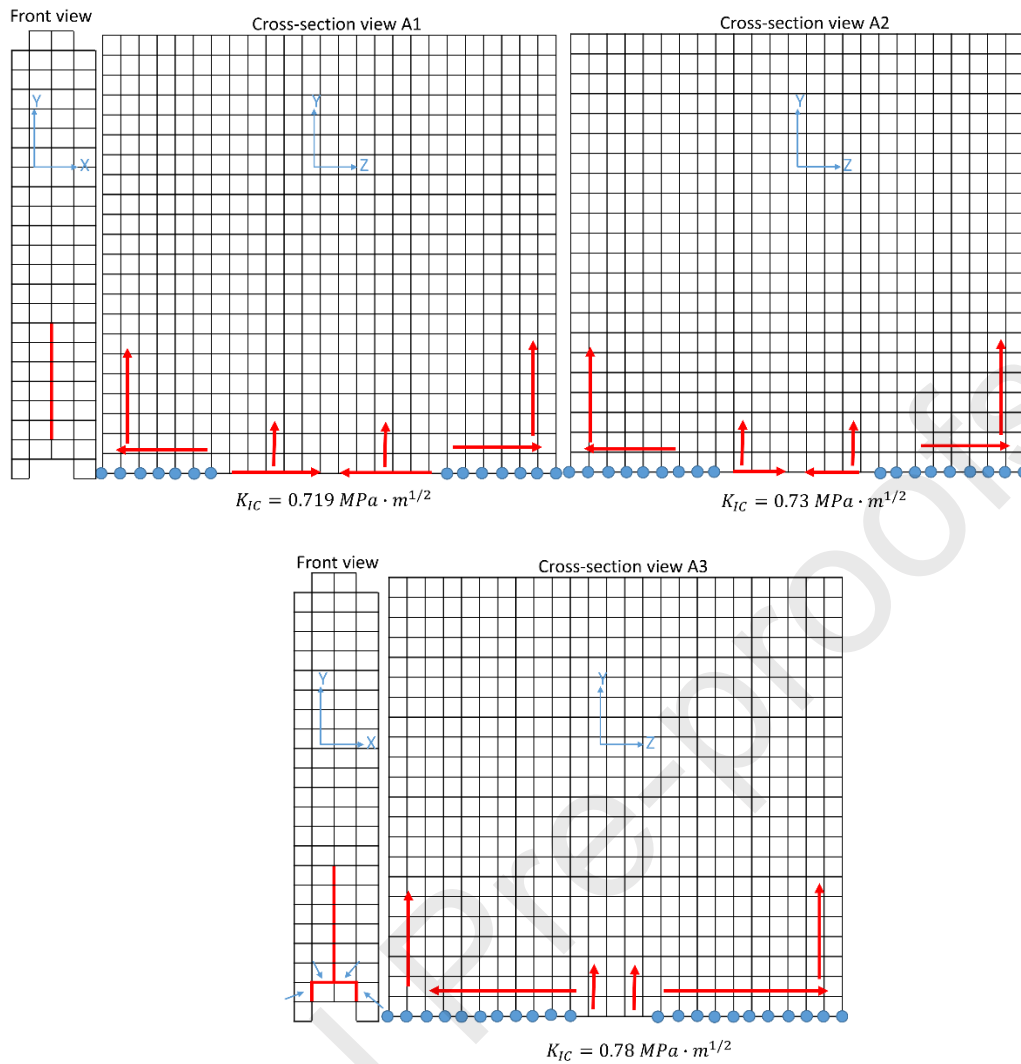


Figure 9 Three cases of the effect of the number of constrained nodes

Furthermore, three different numbers of constrained nodes, i.e., A1, A2 and A3, were also considered in the D4 case with all the constrained nodes gathered at the notch tip, as shown in Figure 9. The increment of the number of constrained nodes was identical from A1 to A2 and from A2 to A3. The focus is on the notch tip as the constrained nodes located further away from this region do not affect the SIF, according to the previous analysis of D1-D4 cases. The increment from A1 to A2 led to a slight increase of the SIF with a straight crack found in the centre of the sample initiated inter-surface, while the SIF in A3 significantly increased compared with A2 due to the presence of branching cracks from the front view (marked by blue arrows in Figure 9, A3), which led to the absorption of more energy and an enhancement of the fracture properties. In summary, Figure 10(a) shows the relationship between the number of constrained nodes and the SIF. A rapid-slow-rapid increase was also obtained as the number of constrained nodes increased. A significant increase occurred when the number of constrained nodes near the crack tip became higher than 18. This phenomenon can be explained by the fact that the fracture property can be efficiently improved as the reinforcement near the crack tip reaches a level that leads to a branching crack and subsequently improves the fracture properties. On the contrary, below

this level, the reinforcement is insufficient to trigger a branching crack. Only one single centre crack is activated, and the resulting increase of the fracture properties by adding nanoparticles is limited.

Herein, the number of the constrained nodes corresponds to the weight fraction of HBP at a macroscale. A larger particle weight fraction produced higher chances of concentrated HBP at the notch tip. Based on Figure 10(a), an illustration of the trend of the fracture properties changing with the weight fraction is presented in Figure 10(b) to explain why the three-stage increase in a rapid-slow-rapid manner was produced with two threshold weight fractions: wf_{t1} and wf_{t2} . The rapid increase of stage 1 was caused by the addition of the nanoparticles. With the reinforcement by nanoparticles at a weight fraction up to 0.1 wt.%, according to the experimental activities [7], the mechanical properties of the nanocomposite can be enhanced compared with the neat polymer. As the weight fraction continued to increase from wf_{t1} , the increase of the fracture properties became slower due to the distribution of the HBP, which was potentially located far from the notch tip and caused little improvement of the fracture properties, marked as stage 2 in Figure 10(b). However, this slow-increase trend started to change after the weight fraction reached wf_{t2} , indicating the beginning of stage 3 with a rapid increase induced by the occurrences of branching cracks. Based on the number of constrained nodes, when the branching cracks initiate in the numerical model while considering the negligible effect of HBP far from the crack tip, wf_{t2} should be larger than 3.0 wt.%. Hence, wf_{t1} and wf_{t2} are of great importance in the application of nanocomposites because guidance can be provided for the material design aiming to improve the fracture properties of epoxy resin with nanoparticles involved. It should be noted that the prediction of these two thresholds can be affected by the accuracy of the numerical model and the limited gradient of the weight fraction in the experiments.

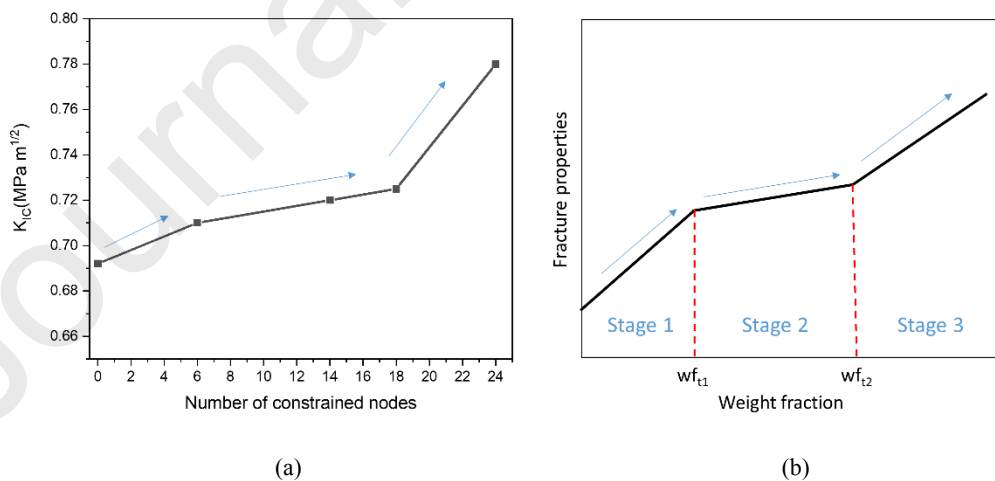


Figure 10 The relationship between the number of constrained nodes and the fracture behaviour from the simulation of the extreme condition (a) and the illustration of the fracture properties changing with the weight fraction (b)

4. Conclusions and future development

A phenomenological modified numerical method in a peridynamic environment was proposed. By randomly constraining the nodes, with a certain number based on the weight fraction, and involving

statistical calculations using Monte Carlo simulations to cover sufficient possible cases, the experimental results from the fracture tests can be successfully captured. Following the validation, the present method was utilised to analyse the effect of the HBP distribution on the fracture properties. With the presented methodology, the distribution of the nanoparticles can be determined on a large scale. Additionally, the numerical procedure provides a more in-depth understanding of the fracture behaviour of such nanocomposites. Indeed, the simulation outcome shows that the increasing trend of the fracture toughness can be attributed to the distribution of the HBP particles, revealing the mechanism behind the observed rapid-slow-rapid increase of fracture properties as a function of particle fraction. A certain level of weight fraction was obtained as the threshold for the rapid increase on the fracture toughness.

However, the proposed methodology, focused on tension-domain fracture modes, has limitations in terms of computational efficiency of the Monte-Carlo simulations and shape of the particle-reinforced nanocomposites, i.e., only sphere-like particles can be considered based on the modification of constraining nodes. However, the current method can also potentially consider other influential factors of such nanocomposites, such as particle-matrix interface property – not only the weight fraction as in the present work, with an alternative modelling technology. As a result, further developments are still expected to enhance the applicability of the methods proposed in the present work.

Acknowledgment

The author Dayou Ma would like to thank Prof. F. Han, from Dalian University of Technology, for the discussion about the application of peridynamics. Support by the Italian Ministry of Education, University and Research, through the project Department of Excellence LIS4.0 (Integrated Laboratory for Lightweight e Smart Structures), is acknowledged.

References

- [1] Nunes SG, Scazzosi R, Manes A, Amico SC, de Amorim Júnior WF, Giglio M. Influence of projectile and thickness on the ballistic behavior of aramid composites: Experimental and numerical study. *Int J Impact Eng* 2019;132:103307. doi:10.1016/j.ijimpeng.2019.05.021.
- [2] Li X, Kupski J, Teixeira De Freitas S, Benedictus R, Zarouchas D. Unfolding the early fatigue damage process for CFRP cross-ply laminates. *Int J Fatigue* 2020;140:105820. doi:10.1016/j.ijfatigue.2020.105820.
- [3] Fu SY, Feng XQ, Lauke B, Mai YW. Effects of particle size, particle/matrix interface adhesion

- and particle loading on mechanical properties of particulate-polymer composites. *Compos Part B Eng* 2008;39:933–61. doi:10.1016/j.compositesb.2008.01.002.
- [4] Liu Y, Cao L, Yuan D, Chen Y. Design of super-tough co-continuous PLA/NR/SiO₂ TPVs with balanced stiffness-toughness based on reinforced rubber and interfacial compatibilization. *Compos Sci Technol* 2018;165:231–9. doi:10.1016/J.COMPSCITECH.2018.07.005.
- [5] Bhanuprakash L, Parasuram S, Varghese S. Experimental investigation on graphene oxides coated carbon fibre/epoxy hybrid composites: Mechanical and electrical properties. *Compos Sci Technol* 2019. doi:10.1016/J.COMPSCITECH.2019.04.034.
- [6] Esmaili A, Sbarufatti C, Ma D, Manes A, Jiménez-Suárez A, Ureña A, et al. Strain and crack growth sensing capability of SWCNT reinforced epoxy in tensile and mode I fracture tests. *Compos Sci Technol* 2019:107918. doi:10.1016/J.COMPSCITECH.2019.107918.
- [7] Zotti A, Elmahdy A, Zuppolini S, Borriello A, Verleysen P, Zarrelli M. Aromatic Hyperbranched Polyester/RTM6 Epoxy Resin for EXTREME Dynamic Loading Aeronautical Applications. *Nanomaterials* 2020;10:188. doi:10.3390/nano10020188.
- [8] Zotti A, Zuppolini S, Borriello A, Zarrelli M. The effect of glassy and rubbery hyperbranched polymers as modifiers in epoxy aeronautical systems. *Compos Part B Eng* 2019;169:88–95. doi:10.1016/j.compositesb.2019.04.006.
- [9] Verrey J, Winkler Y, Michaud V, Månson JAE. Interlaminar fracture toughness improvement in composites with hyperbranched polymer modified resin. *Compos Sci Technol* 2005;65:1527–36. doi:10.1016/j.compscitech.2005.01.005.
- [10] DeCarli M, Kozielski K, Tian W, Varley R. Toughening of a carbon fibre reinforced epoxy anhydride composite using an epoxy terminated hyperbranched modifier. *Compos Sci Technol* 2005;65:2156–66. doi:10.1016/j.compscitech.2005.05.003.
- [11] Boogh L, Pettersson B, Månson JAE. Dendritic hyperbranched polymers as tougheners for epoxy resins. *Polymer (Guildf)* 1999;40:2249–61. doi:10.1016/S0032-3861(98)00464-9.
- [12] Buonocore GG, Schiavo L, Attianese I, Borriello A. Hyperbranched polymers as modifiers of epoxy adhesives. *Compos Part B Eng* 2013;53:187–92. doi:10.1016/j.compositesb.2013.04.062.
- [13] Pilla S, Kramschuster A, Lee J, Clemons C, Gong S, Turng LS. Microcellular processing of polylactide-hyperbranched polyester-nanoclay composites. *J Mater Sci* 2010;45:2732–46. doi:10.1007/s10853-010-4261-6.
- [14] Li S, Yao Y. Synergistic improvement of epoxy composites with multi-walled carbon nanotubes and hyperbranched polymers. *Compos Part B Eng* 2019;165:293–300.

- doi:10.1016/j.compositesb.2018.11.122.
- [15] Maier M, Alstädt V, Vinckier D, Thoma K. Numerical and experimental analysis of the compact tension test for a group of modified epoxy resins. *Polym Test* 1994;13:55–66. doi:10.1016/0142-9418(94)90040-X.
- [16] Ma D, Esmaili A, Manes A, Sbarufatti C, Jiménez-Suárez A, Giglio M, et al. Numerical study of static and dynamic fracture behaviours of neat epoxy resin. *Mech Mater* 2020;140:103214. doi:10.1016/J.MECHMAT.2019.103214.
- [17] Esmaili A, Ma D, Manes A, Oggioni T, Jiménez-Suárez A, Urena A, et al. An experimental and numerical investigation of highly strong and tough epoxy based nanocomposite by addition of MWCNTs: Tensile and mode I fracture tests. *Compos Struct* 2020:112692. doi:10.1016/j.compstruct.2020.112692.
- [18] Ma D, Giglio M, Manes A. An investigation into mechanical properties of the nanocomposite with aligned CNT by means of electrical conductivity. *Compos Sci Technol* 2020;188:107993. doi:10.1016/J.COMPSCITECH.2020.107993.
- [19] Arsenidis P, Karatasos K. Computational Study of the Interaction of a PEGylated Hyperbranched Polymer/Doxorubicin Complex with a Bilipid Membrane. *Fluids* 2019;4:17. doi:10.3390/fluids4010017.
- [20] Das S, Hoffarth C, Ren B, Spencer B, Sant G, Rajan SD, et al. Simulating the Fracture of Notched Mortar Beams through Extended Finite-Element Method and Peridynamics. *J Eng Mech* 2019;145:04019049. doi:10.1061/(ASCE)EM.1943-7889.0001628.
- [21] Frankland SJ V, Caglar A, Brenner DW, Griebel M. Molecular Simulation of the Influence of Chemical Cross-Links on the Shear Strength of.pdf 2002:3046–8.
- [22] Meng Z, Bessa MA, Xia W, Kam Liu W, Keten S. Predicting the Macroscopic Fracture Energy of Epoxy Resins from Atomistic Molecular Simulations. *Macromolecules* 2016;49:9474–83. doi:10.1021/acs.macromol.6b01508.
- [23] Silling SA. Reformulation of elasticity theory for discontinuities and long-range forces. *J Mech Phys Solids* 2000;48:175–209. doi:10.1016/S0022-5096(99)00029-0.
- [24] Ren B, Wu CT, Askari E. A 3D discontinuous Galerkin finite element method with the bond-based peridynamics model for dynamic brittle failure analysis. *Int J Impact Eng* 2017;99:14–25. doi:10.1016/j.ijimpeng.2016.09.003.
- [25] Mitts C, Naboulsi S, Przybyla C, Madenci E. Axisymmetric peridynamic analysis of crack deflection in a single strand ceramic matrix composite. *Eng Fract Mech* 2020;235:107074.

- doi:10.1016/j.engfracmech.2020.107074.
- [26] Wu P, Zhao J, Chen Z, Bobaru F. Validation of a stochastically homogenized peridynamic model for quasi-static fracture in concrete. *Eng Fract Mech* 2020;237:107293. doi:10.1016/j.engfracmech.2020.107293.
- [27] Genckal N, Seidel GD. Multiscale Modeling of Damage Response in Nanocomposites Reinforced with Carbon Nanotubes. *AIAA Scitech 2020 Forum* 2020:1–12. doi:10.2514/6.2020-1380.
- [28] Han F, Azdoud Y, Lubineau G. Computational modeling of elastic properties of carbon nanotube/polymer composites with interphase regions. Part II: Mechanical modeling. *Comput Mater Sci* 2014;81:652–61. doi:10.1016/j.commatsci.2013.07.008.
- [29] Zotti A, Zuppolini S, Borriello A, Zarrelli M. Survey data on thermal properties of different hyperbranched polymers (HBPs) and on morphological and thermal analysis of the corresponding epoxy matrix nanocomposites. *Data Br* 2019;25:104303. doi:10.1016/J.DIB.2019.104303.
- [30] Silling SA, Epton M, Weckner O, Xu J, Askari E. Peridynamic states and constitutive modeling. *J Elast* 2007;88:151–84. doi:10.1007/s10659-007-9125-1.
- [31] Ren B, Wu CT. A Peridynamic Model for Damage Prediction of Fiber-reinforced Composite Laminate. 15 th Int. LS-DYNA ® Users Conf., 2018.
- [32] Ahmadi M, Hosseini-Toudeshky H, Sadighi M. Peridynamic micromechanical modeling of plastic deformation and progressive damage prediction in dual-phase materials. *Eng Fract Mech* 2020;235:107179. doi:10.1016/j.engfracmech.2020.107179.
- [33] Nguyen CT, Oterkus S, Oterkus E. An energy-based peridynamic model for fatigue cracking. *Eng Fract Mech* 2020:107373. doi:10.1016/j.engfracmech.2020.107373.
- [34] Mehrmashhadi J, Bahadori M, Bobaru F. On validating peridynamic models and a phase-field model for dynamic brittle fracture in glass. *Eng Fract Mech* 2020;240:107355. doi:10.1016/j.engfracmech.2020.107355.
- [35] Wu CT. Kinematic constraints in the state-based peridynamics with mixed local/nonlocal gradient approximations. *Comput Mech* 2014;54:1255–67. doi:10.1007/s00466-014-1055-8.
- [36] Zhan JM, Yao XH, Han F. An approach of peridynamic modeling associated with molecular dynamics for fracture simulation of particle reinforced metal matrix composites. *Compos Struct* 2020:112613. doi:10.1016/j.compstruct.2020.112613.
- [37] Zhao J, Chen Z, Mehrmashhadi J, Bobaru F. A stochastic multiscale peridynamic model for

corrosion-induced fracture in reinforced concrete. Eng Fract Mech 2020:106969.
doi:10.1016/J.ENGFRACTMECH.2020.106969.

- [38] Standard Test Methods for Plane-Strain Fracture Toughness and Strain Energy Release Rate of Plastic Materials BT - Standard Test Methods for Plane-Strain Fracture Toughness and Strain Energy Release Rate of Plastic Materials 2014.
- [39] Broek D. The practical use of fracture mechanics. Springer Science & Business Media; 2012.

Journal Pre-proofs

A modified peridynamic method to model the fracture behaviour of nanocomposites

Dayou Ma^{a*}, Patricia Verleysen^b, Sarath Chandran^b, Marco Giglio^a, Andrea Manes^a

^a Politecnico di Milano, Department of Mechanical Engineering, via la Masa 1, 20156 Milan, Italy. dayou.ma@polimi.it, marco.giglio@polimi.it, andrea.manes@polimi.it.

^b Department of Electromechanical, Systems & Metal Engineering, MST-DyMaLab, Ghent University, Technologiepark 46, B-9052 Zwijnaarde, Belgium. patricia.verleysen@UGent.be, sarath.chandran@UGent.be

* Corresponding author: Dayou Ma, dayou.ma@polimi.it.

HIGHLIGHTS:

- Peridynamic method is used to replicate the fracture behaviours of nanocomposites: epoxy resin with HBP.
- The presence of nanoparticles, HBP, is simulated at macroscale by constrained nodes.
- A rapid-slow-rapid increasing trend of fracture toughness for nanocomposites is obtained with the increase of the weight fraction of HBP.
- Effect of HBP particles' distribution on the fracture behaviour is investigated.

A modified peridynamic method to model the fracture behaviour of nanocomposites (HBP/RTM-6 resin)

Dayou Ma^{a*}, Patricia Verleysen^b, Sarath Chandran^b, Marco Giglio^a, Andrea Manes^a

^a Politecnico di Milano, Department of Mechanical Engineering, via la Masa 1, 20156 Milan, Italy. dayou.ma@polimi.it, marco.giglio@polimi.it, andrea.manes@polimi.it.

^b Department of Electromechanical, Systems & Metal Engineering, MST-DyMaLab, Ghent University, Technologiepark 46, B-9052 Zwijnaarde, Belgium. patricia.verleysen@UGent.be, sarath.chandran@UGent.be

* *Corresponding author: Dayou Ma, dayou.ma@polimi.it.*

All authors state that:

- All authors have participated in (a) conception and design, or analysis and interpretation of the data; (b) drafting the article or revising it critically for important intellectual content; and (c) approval of the final version.
- This manuscript has not been submitted to, nor is under review at, another journal or other publishing venue.
- The authors have no affiliation with any organization with a direct or indirect financial interest in the subject matter discussed in the manuscript